2013 European Control Conference (ECC)
July 17-19, 2013, Zürich, Switzerland.

State-space Modelling of Hysteresis-based Control Schemes

Soumya Kundu Ian A. Hiskens

***Abstract*— The paper develops a state-space model for the aggregate power drawn by a group of plug-in electric vehicle (PEV) chargers under hysteresis-based charging. The aggregate response of the PEV charging loads to changes in the hysteresis deadband is nonlinear, requiring detailed analysis to accurately capture the dynamics. Related work, which focused on thermostatically controlled loads (TCLs), addressed state-space modelling by dividing the hysteresis deadband into equally sized bins and keeping track of the inter-bin migration of loads. A system of PEV chargers can be treated similarly. A new modelling paradigm has been developed to allow for fast variation of the hysteresis deadband. This model tracks the distribution of PEV chargers within the hysteresis deadband, with the inter-bin migration of chargers used to capture the aggregate dynamics.**

I. Introduction

Hysteresis-based processes underpin the control of many electrical loads, particularly those that involve thermostats, for example air-conditioner and water heaters. While hysteresis-based control is not natural for charging the batteries of plug-in electric vehicles (PEVs), it has been shown in [1], [2] that by establishing a nominal charging profile and a surrounding deadband, charging can be formulated as a hysteresis-based mechanism. An illustration is provided in Fig. 1.

Numerous studies have shown that useful control laws can be designed so that the aggregate power demanded by a group of hysteresis-based electrical loads follows certain desired trajectories [1]-[8]. To design a good control law, it is important to completely understand the dynamic behaviour of the aggregated load group. A necessary step is the development of a state-space model that accurately captures the response of the population to a wide range of controlled variations of the hysteresis band.

A Fokker-Planck model was derived in [9] to capture the aggregate dynamics of a population of thermostats. It was shown in [3] that the probability of thermostatic loads being ON (drawing power) or OFF (not drawing any power) can be estimated rather accurately for a large population. More recent work has shown that population dynamics can be modelled by dividing the hysteresis band into several equal-sized bins and keeping track of the movement of thermostats from one bin to another [4], [5], [6]. An alternative, linearized input-output transfer function model was developed in [2]

S. Kundu and I.A. Hiskens are with the Department of Electrical Engineering and Computer Science, University of Michigan, Ann Arbor, USA, (soumyak,hiskens@umich.edu).

Research supported by the National Science Foundation through EFRI-RESIN grant 0835995, and the Department of Energy through the Clean Energy Research Centre for Clean Vehicle Collaboration (CERC-CVC), award number DE-PI0000012.

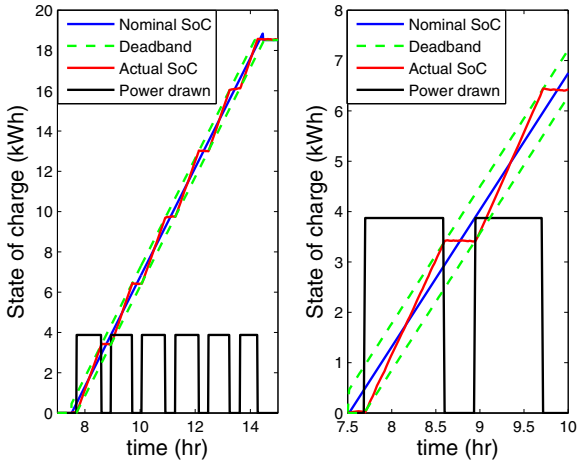

Fig. 1. Hysteresis-based PEV charging strategy.

for the hysteresis-based PEV charging strategy proposed in [1]. However the aggregate response of PEV charging load to changes in the position of the hysteresis band is inherently nonlinear, hence the need for detailed analysis to capture the holistic dynamics.

The paper considers a hysteresis-based control strategy for regulating the power demand of a homogeneous population of PEV chargers. A state-space model is developed to accurately represent the system response to changes in the deadband position. Section II briefly introduces the hysteresis-based charging process. The modelling approach is described in Section III, while Section IV presents simulation results that explore the capabilities of the developed model over a wide range of control signals. Conclusions are presented in Section V.

II. System Description

In modelling the aggregate demand of a group of PEV chargers, a homogeneous noise-free system will be considered. A typical hysteresis-based charging profile is shown in Fig. 1, where the state-of-charge (SoC) always remains within the deadband established around the nominal SoC profile. By making the deadband width of each PEV charger proportional to its maximum charge requirement E_{max}, the SoC can be normalized such that the corresponding normalized deadband is symmetric around zero [2]. The dynamics of the resulting normalized SoC can be expressed as,

$$\dot{\widetilde{SoC}}(t) = \frac{s(t)P_{max} - P_{nom}}{E_{max}} \tag{1a}$$

TABLE I

KEY SYMBOLS

N_v	number of PEVs
N	number of bins into which the deadband is divided
SoC	state-of-charge (kWh)
$\widetilde{SoC}$	normalized state-of-charge (SoC)
P_{max}	maximum charging rate (kW)
P_{nom}	nominal charging rate (kW)
E_{max}	battery charge capacity (kWh)
Δ	deadband width as a fraction of battery capacity
$x_i(t)$	probability density of chargers in i^{th} bin
$u(t)$	shift in normalized SoC deadband over time
$v(t)$	rate at which normalized SoC deadband changes

where

$$\dot{s} = 0 \quad \text{while} \quad -\Delta/2 < \widetilde{SoC}(t) < \Delta/2 \tag{1b}$$

and

$$s(t^+) = \begin{cases} s(t)+1 & \text{when } \widetilde{SoC}(t) = -\Delta/2 \\ s(t)-1 & \text{when } \widetilde{SoC}(t) = \Delta/2, \end{cases} \tag{1c}$$

with t^+ denoting the time instant immediately following the switching induced by $\widetilde{SoC}$ reaching the upper or lower limit of the (normalized) deadband. With this formulation, the width of the deadband becomes Δ. It is also useful to define the two parameters α_{on} and α_{off} as the rate of increase and decrease of $\widetilde{SoC}$, respectively. From (1a) ,

$$\alpha_{on} := \frac{(P_{max} - P_{nom})}{E_{max}} \tag{2}$$

$$\alpha_{off} := -\frac{P_{nom}}{E_{max}}. \tag{3}$$

The remainder of the paper focuses on the normalized deadband and normalized SoC. For brevity, the qualifier "normalized" will subsequently be dropped.

III. MODELLING AGGREGATE DYNAMICS

A. All chargers inside the hysteresis band

If any PEV chargers are initially outside the (normalized) deadband, then the dynamics of (1) will force them to move inside. Once a charger is inside the deadband, it will remain inside unless the deadband moves quickly, as discussed in Section III-B, or charging is completed.

One approach to capturing the aggregate dynamics of a population of hysteresis-based PEV chargers is to divide the deadband into N sections of equal width,

$$\delta_{bin} := \Delta/N, \tag{4}$$

and quantify the migration of chargers from one bin to another [4], [5]. At any moment, some of the chargers within the deadband will be in the ON-state while the rest will be in the OFF-state. It is therefore useful to consider N bins of equal width each holding a (not necessarily equal) number of ON chargers and another N bins each holding a number of OFF chargers. The number of chargers in each of those $2N$ bins describes the probability distribution of SoC across the population. Fig. 2 provides an illustration. The height of

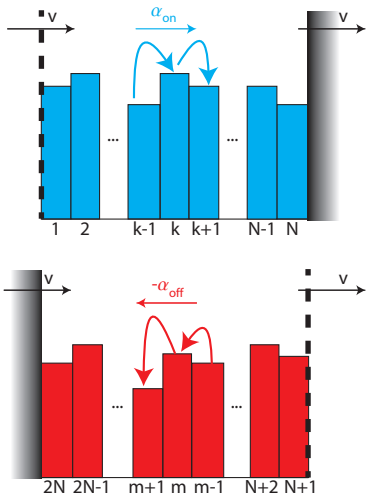

Fig. 2. Inter-bin migration when all the loads are inside the deadband.

a bin represents the probability density of chargers in that bin. Let the height of the i-th bin at time t be given by $x_i(t)$, $i = 1,\ldots,2N$. The probability that a PEV lies within the i-th bin is then $x_i(t)\delta_{bin}$, and hence,

$$\delta_{bin} \sum_{i=1}^{2N} x_i(t) = 1. \tag{5}$$

Bins numbered 1 to N account for the ON-state chargers while bins numbered $N+1$ to $2N$ account for the OFF-state chargers. The chargers in the ON-state move to the right (as their SoC increases) at a speed α_{on} and the OFF-state chargers move to the left at a rate α_{off}. The dynamic model (1) ensures that no ON-state chargers can exist to the right of the upper deadband limit, while no OFF-state chargers may exist to the left of the lower deadband limit. Any ON-state chargers hitting the upper deadband limit instantly switch to the OFF-state, and any OFF-state chargers that encounter the lower deadband limit switch to the ON-state.

1) Static deadband: To start with, the deadband is assumed to be static, i.e. the control action $u(t)$ describing the shift in the deadband is zero. As discussed in [4], the change in probability density $x_i(t)$ is nothing but the difference between the inflow of chargers from the $(i-1)$-th bin and the outflow of chargers from the i-th bin, for $i = 2,\ldots,2N$. For $i = 1$, the inflow is from the $2N$-th bin. Taking care of the switching at the two deadband limits, the dynamics can be written,

$$\dot{x}_i(t)\delta_{bin} = \begin{cases} -x_{2N}(t)\alpha_{off} - x_1(t)\alpha_{on}, & i = 1 \\ \big(x_{i-1}(t) - x_i(t)\big)\alpha_{on}, & i = 2,\ldots,N \\ x_N(t)\alpha_{on} + x_{N+1}(t)\alpha_{off}, & i = N+1 \\ -\big(x_{i-1}(t) - x_i(t)\big)\alpha_{off}, & i = N+2,\ldots,2N. \end{cases} \tag{6}$$

The total power demand is given by,

$$P_{tot}(t) = N_v P_{max}\delta_{bin} \sum_{i=1}^{N} x_i(t). \tag{7}$$

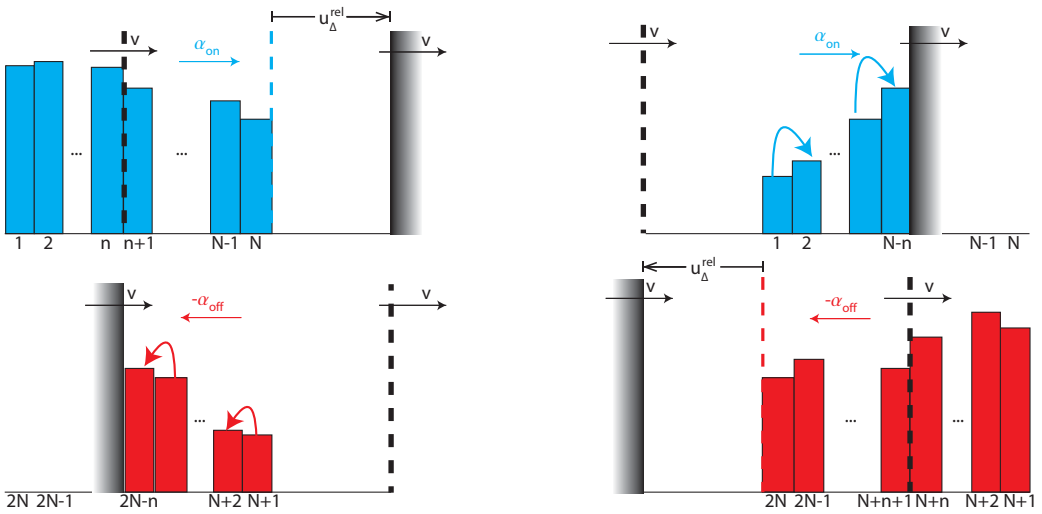

(a) Chargers lie left of the lower deadband limit

(b) Chargers lie right of the upper deadband limit

Fig. 3. Inter-bin migration when some of the chargers lie outside the deadband limits.

Note that the $N+1,\ldots,2N$ bins correspond to OFF-state chargers and hence do not contribute to instantaneous power demand.

2) Slowly moving deadband: The above description holds when the deadband is static. However if the deadband moves, under the influence of a control signal $u(t)$, then it is necessary to reconsider the meaning of the bins. As before, the deadband is still divided into N bins of equal width δ_{bin}, but now those bins move with the deadband. The SoC range associated with each bin is no longer defined in absolute terms, but rather is defined relative to the moving deadband. Consequently, if control $u(t)$ causes the deadband to move at a rate $\frac{du(t)}{dt} \equiv v(t)$, then the effective rate at which inter-bin migrations take place will change. For example, if the deadband limits move with a rate $v = \alpha_{on}/2$ in the same direction as α_{on}, as illustrated in Fig. 2, the effective rate at which the ON-state chargers in the N-th bin hit the upper limit will be $\alpha_{on}/2$ and the rate at which OFF-state chargers in the $2N$-th bin hit the lower deadband limit will be $\alpha_{on}/2 - \alpha_{off}$.

If the rate $v(t)$ at which the deadband limits move has a magnitude that is less than the natural rates[1] α_{on} and $-\alpha_{off}$, then the migrations will continue to occur, but with adjusted rates $\alpha_{on} - v(t)$ and $-\alpha_{off} + v(t)$ instead of α_{on} and $-\alpha_{off}$, respectively. Consequently, the dynamics of migration in (6) become,

$$\dot{x}_i(t)\delta_{bin} = \begin{cases} -x_{2N}(t)(\alpha_{off} - v(t)) - x_1(t)(\alpha_{on} - v(t)), & i = 1 \\ \big(x_{i-1}(t) - x_i(t)\big)\big(\alpha_{on} - v(t)\big), & i = 2,\ldots,N \\ x_N(t)\big(\alpha_{on} - v(t)\big) + x_{N+1}(t)\big(\alpha_{off} - v(t)\big), & i = N+1 \\ -\big(x_{i-1}(t) - x_i(t)\big)\big(\alpha_{off} - v(t)\big), & i = N+2,\ldots,2N \end{cases} \tag{8}$$

[1]Recall $\alpha_{off} < 0$ by definition (3).

with total power given by (7). The existence of terms such as $x_i(t)v(t)$ in the right-hand side of (8) indicates that the resulting state-space model is bilinear [4].

It is anticipated that the state-space model will become more complicated when the deadband moves quickly. While the rate of change of the deadband is relatively slow, $\alpha_{off} < v(t) < \alpha_{on}$, chargers will continue encountering the upper and lower limits of the hysteresis band, the right boundary for ON-state chargers and the left boundary for OFF-state chargers. As a result, all of the chargers will remain inside the deadband even as it moves. However, if the deadband varies at a sufficiently high rate, switching between states will no longer operate according to (8). In particular, if the deadband moves towards the right with a speed $v(t) > \alpha_{on}$, switching at the upper deadband limit will no longer occur, though the OFF-state chargers will continue to encounter the lower deadband limit, with a rate $v(t) - \alpha_{off}$. Consequently, over time the N-th bin will lag behind the upper deadband limit and will separate from it. This is illustrated in Fig. 3(a). Furthermore, some of the ON-state chargers will now lie outside the deadband, to the left of the lower limit. An equivalent situation occurs when $v(t) < \alpha_{off}$, as illustrated in Fig. 3(b). In this case, the $2N$-th bin and the lower deadband limit will become separated, and some of the OFF-state chargers will lie to the right of the upper deadband limit.

B. Chargers lying outside the hysteresis band

In considering this case, it is assumed that initially all the chargers were inside the deadband and as the deadband moved faster than the natural rates α_{on} and $-\alpha_{off}$, some or all of the chargers fell behind the shifted deadband. Fig. 3(a) shows a typical case where the deadband has moved quickly to the right, and some of the ON-state chargers now lie to the left of the lower deadband limit. Considering the dynamics in (8), it can be seen that as $v(t)$ increases and approaches α_{on}, the rate of inter-bin migration of ON-state chargers, proportional to $\alpha_{on} - v(t)$, decreases. As $v(t)$

increases beyond α_{on}, the inter-bin migration within the ON-state, and the ON- to OFF-state switching at the right boundary, both stop. A "gap" is created between the N-th bin and the right boundary. An equivalent situation occurs for the OFF-state when $v(t)$ decreases faster than α_{off}, as shown in Fig. 3(b).

The "gap" between the extreme end bin and the upper or lower boundary can be quantified using the variable u_{Δ}^{rel}, as shown in Fig. 3. When $u(t)$ varies continuously, so that $v(t)$ is finite, the behaviour of u_{Δ}^{rel} is governed by the switched dynamical system:

$$\frac{du_{\Delta}^{rel}}{dt} = y(t) \tag{9a}$$

where

$$y(t) = \begin{cases} v(t)-\alpha_{on}, & \left(u_{\Delta}^{rel}(t)=0 \wedge v(t) \geq \alpha_{on}\right) \vee u_{\Delta}^{rel}(t) > 0 \\ v(t)-\alpha_{off}, & \left(u_{\Delta}^{rel}(t)=0 \wedge v(t) \leq \alpha_{off}\right) \vee u_{\Delta}^{rel}(t) < 0 \\ 0, & \text{otherwise} \end{cases} \tag{9b}$$

and $\wedge$ and $\vee$ denote standard Boolean operators. With all chargers initially inside the deadband limits, the gap $u_{\Delta}^{rel}(t)$ will remain zero while the rate $v(t)$ at which the deadband varies remains within the natural rates at which SoC varies, i.e. $\alpha_{off} < v(t) < \alpha_{on}$. If $v(t)$ deviates beyond those bounds, then $u_{\Delta}^{rel}(t)$ will become non-zero, implying that some bins lie outside the deadband. Bins will lie below the lower deadband limit if $u_{\Delta}^{rel}(t) > 0$, as illustrated in Fig. 3(a). Fig. 3(b) shows that for $u_{\Delta}^{rel}(t) < 0$, bins will lie above the upper deadband limit.

If $u(t)$ undergoes a step change, then $v(t)$ will be undefined at that instant and (9) is no longer applicable. To resolve this difficulty, the input signal can be decomposed into a component $u(t)$ that varies continuously and a component $\Delta u(t)$ that is constant apart from step changes. The continuous component $u(t)$ establishes $v(t)$, and thus drives variations in $u_{\Delta}^{rel}(t)$ according to (9). To account for the step-wise contribution given by $\Delta u(t)$, the total variation in $u_{\Delta}^{rel}(t)$ is given by,

$$u_{\Delta}^{rel}(t) = u_{\Delta(9)}^{rel}(t) + \Delta u(t) \tag{10}$$

where $u_{\Delta(9)}^{rel}(t)$ refers to the value of $u_{\Delta}^{rel}(t)$ given by (9).

The number of bins (either ON or OFF) lying outside the deadband is nominally given by $u_{\Delta}^{rel}(t)/\delta_{bin}$. This will generically result in a non-integer number of bins though. To overcome this difficulty, bins that straddle a deadband limit will be treated as lying entirely outside the deadband. Accordingly, the number of bins outside the deadband at time t is given by,

$$n_t := \min\left(\left\lceil \frac{\left|u_{\Delta}^{rel}(t)\right|}{\delta_{bin}} \right\rceil, N \right). \tag{11}$$

The approximation inherent in rounding up, as achieved by the "ceiling" function in (11), is incidental as the width of a bin is a small fraction, $1/N$, of the deadband width.

A general purpose model must be able to quantify the inter-bin migration of chargers for situations such as those depicted in Fig. 3. In Section III-A, the deadband was divided into N equal bins, with (8) describing the evolution of chargers within those bins. This resulted in a state-space of dimension $2N$. It is natural to consider increasing the number of bins to cover the possibility of chargers lying outside the deadband. However, this would require a larger state-space, and might result in scalability and/or computational issues if the shifts in deadband had the potential to be large. It will be shown that stretching the state-space is not necessary, with $2N$ states able to capture the dynamics under all situations.

1) Chargers lying left of the lower limit, $u_{\Delta}^{rel}(t) > 0$: Consider the case when some (or all) of the chargers are lying to the left of the lower deadband limit. There is a gap between the right-most ON-state charger and the upper deadband limit, as illustrated in Fig. 3(a). Thus no chargers will encounter the upper limit, and hence no switching from the ON- to the OFF-state will occur. Consequently all the ON-state bins must move towards the right with the common natural rate α_{on}, and so no inter-bin migration will occur between any of the ON-state bins. However, switching from the OFF- to the ON-state at the lower limit will continue, thereby increasing the height of the ON-state bin that coincides with the lower deadband limit.

When all the chargers were inside the deadband limits (Section III-A) the bins were referenced relative to the deadband. Even though the deadband moved at $v(t) \in (\alpha_{off}, \alpha_{on})$, the bin positions relative to the deadband remained fixed. In the case when chargers lie to the left of the lower deadband limit, the ON-state bin positions can be chosen as reference. That is, the ON-state bins remain fixed and the deadband moves with relative rate $v(t)-\alpha_{on}$. Consequently, the SoC of the OFF-state chargers vary at the relative rate $\alpha_{off}-\alpha_{on}$. Due to the absence of any boundary switching from the ON- to the OFF-state, the height of the $(N+1)$-th bin in the OFF-state will simply decrease at a rate proportional to $(\alpha_{on}-\alpha_{off})x_{N+1}(t)$. The rate of OFF- to ON-state switching is proportional to $x_{2N-n_t}(t)\max\big(0, v(t)-\alpha_{off}\big)$, where n_t is given by (11). This takes into account that if $v(t) < \alpha_{off}$ there can be no switching from the OFF- to the ON-state. The state dynamics for all bins can be summarized as:

$$\dot{x}_i(t)\delta_{bin} = \begin{cases} x_{2N-n_t}(t)\max\big(0, v(t)-\alpha_{off}\big), & i = n_t+1 \\ x_i(t)(\alpha_{off}-\alpha_{on}), & i = N+1 \\ -\big(x_{i-1}(t)-x_i(t)\big)(\alpha_{off}-\alpha_{on}), & i = N+2,..,2N-n_t-1 \\ -x_i(t)\max\big(0, v(t)-\alpha_{off}\big) & \\ \qquad -x_{i-1}(t)(\alpha_{off}-\alpha_{on}), & i = 2N-n_t \\ 0, & \text{all other } i. \end{cases} \tag{12}$$

2) Chargers lying right of the upper limit, $u_{\Delta}^{rel}(t) < 0$: When some or all of the chargers lie to the right of the upper deadband limit, as illustrated in Fig. 3(b), a formulation similar to that in Section III-B.1 can be established, though

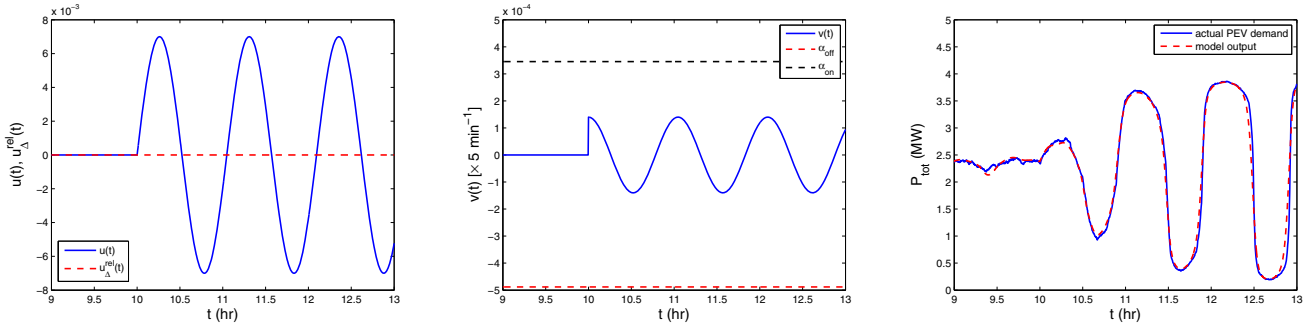

(a) (b) (c)

Fig. 4. Case 1, corresponding to Section III-A. The deadband moves slowly and all chargers remain within the limits.

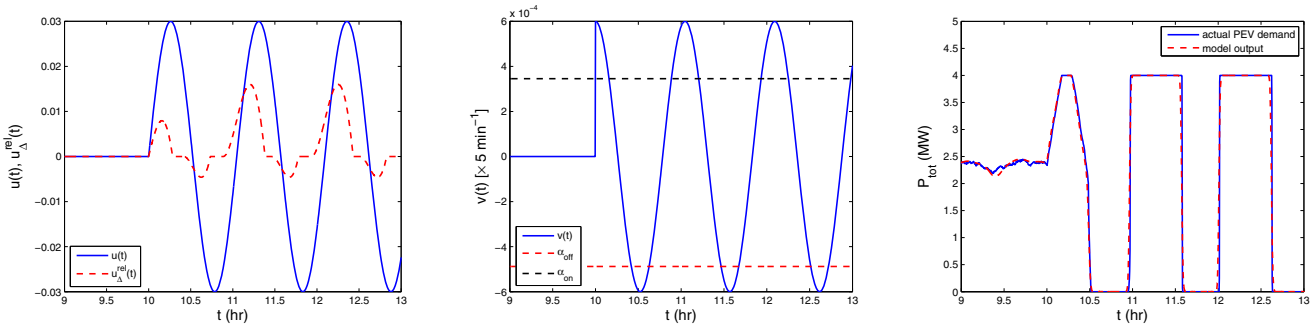

(a) (b) (c)

Fig. 5. Case 2, corresponding to Section III-B. The deadband moves rapidly and some chargers fall outside the limits.

in this case the OFF-state bins provide the reference. With this reference, the SoC of the OFF-state chargers remains constant, with no inter-bin migration occurring. The SoC of the ON-state chargers varies at the rate $\alpha_{on}-\alpha_{off}$, however. Also, the ON- to OFF-state switching at the right deadband limit is proportional to $x_{N-n_t}(t)\max\big(0,(\alpha_{on}-v(t))\big)$, where n_t is the number of OFF-state bins lying to the right of the upper deadband limit at time t, as given by (11). The state equations become:

$$\dot{x}_i(t)\delta_{bin} = \begin{cases} -x_i(t)(\alpha_{on}-\alpha_{off}), & i=1 \\ \big(x_{i-1}(t)-x_i(t)\big)(\alpha_{on}-\alpha_{off}), & i=2,\ldots,N-n_t-1 \\ -x_i(t)\max\big(0,\alpha_{on}-v(t)\big) & \\ \qquad +x_{i-1}(t)(\alpha_{on}-\alpha_{off}), & i=N-n_t \\ x_{N-n_t}(t)\max\big(0,\alpha_{on}-v(t)\big), & i=N+n_t+1 \\ 0, & \text{all other } i. \end{cases} \tag{13}$$

IV. Simulation

The model built in Section III has been compared with Monte-Carlo simulation of a homogeneous population of PEV chargers[2], each governed by the dynamics of (1). Fig. 4 illustrates a situation where the deadband moves slowly. Fig. 4(a) shows that the deadband oscillates sinusoidally, while Fig. 4(b) confirms that the rate of movement stays within $(\alpha_{off},\alpha_{on})$. Given this slow movement, $u_\Delta^{rel}(t)$ equals zero throughout, as seen in Fig. 4(a), and all the chargers remain inside the deadband limits. The resulting aggregate power demand is shown in Fig. 4(c). It can be seen that the model output closely matches the Monte-Carlo simulation.

The second case considers fast movement of the deadband, and is illustrated in Fig. 5. The deadband position $u(t)$, shown in Fig. 5(a), moves faster than the natural SoC rates, and as a result, $v(t)$ deviates outside the range $(\alpha_{off},\alpha_{on})$. This is shown in Fig. 5(b). Some chargers start to fall outside the deadband limits, with Fig. 5(a) showing that $u_\Delta^{rel}(t)$ takes on non-zero values. At the instant when $v(t)$ increases beyond α_{on}, the relative "gap" between the bins and the deadband $u_\Delta^{rel}(t)$ becomes positive. It remains so until after $v(t)$ has dropped below α_{on} and the bins have caught up with the deadband limits. Fig. 5(c) shows that the aggregate demand undergoes large oscillations, with fluctuations ranging between the maximum demand, when all PEVs are charging, and zero.

In the third case, presented in Fig. 6, the deadband is forced to undergo high-frequency pulses, followed by a much slower sinusoidal oscillation. The input signal $u(t)$ and corresponding "gap" measure u_Δ^{rel} are provided in Fig. 6(a). Fig. 6(b) shows that even after the deadband movement slows down, the total power continues to oscillate between the maximum and zero, though with a reduced frequency. Thus

[2]Referring to Table I, parameters for the simulation are: $N_v=1000$, $N=200$, $\Delta=0.05$, $P_{max}=4$ kW, $P_{nom}=2.4$ kW, $E_{max}=16$ kW-hr. The continuous dynamics of (1) was discretized using a time-step of 0.2 min.

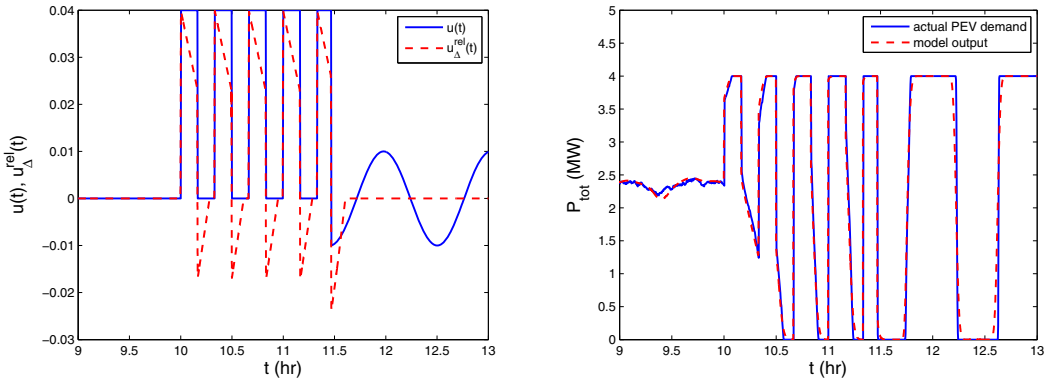

(a) (b)

Fig. 6. Case 3, high-frequency deadband movement renders the system less responsive to slow variations.

exposure to high frequency, and relatively large, movements in the deadband position can synchronize chargers, rendering the system almost unresponsive to subsequent small and slow changes in the deadband position.

V. Conclusions

The paper has considered a hysteresis-based charging process that enables regulation of the aggregate power demand of a large population of PEVs. To achieve control, the hysteresis band of all PEVs is adjusted by a common input signal. A detailed nonlinear state-space model has been developed to capture the aggregate population dynamics in response to deadband movement. The model is able to accurately replicate dynamic behaviour even in the presence of very large fluctuations in the deadband position. It provides the basis for exploring system response to a wide range of control actions. The modelling approach is not restricted to populations of PEV chargers. It is just as applicable to other hysteresis-based processes, such as thermostatically controlled loads.

References

[1] D. S. Callaway and I. A. Hiskens, "Achieving Controllability of Electric Loads," *Proceedings of IEEE*, vol. 99, no. 1, pp. 184–199, Jan. 2011.

[2] S. Kundu and I. A. Hiskens, "Hysteresis-based Charging Control of Plug-in Electric Vehicles," *51st IEEE Conference on Decision and Control*, Dec. 2012.

[3] D. S. Callaway, "Tapping the energy storage potential in electric loads to deliver load following and regulation, with application to wind energy," *Energy Conversion and Management*, vol. 50, no. 5, pp. 1389–1400, May 2009.

[4] S. Bashash and H. K. Fathy, "Modeling and Control Insights into Demand-side Energy Management through Setpoint Control of Thermostatic Loads," *American Control Conference*, pp. 4546 – 4553, 2011.

[5] F. Koch, J. L. Mathieu, and D. S. Callaway, "Modeling and control of aggregated heterogeneous thermostatically controlled loads for ancillary services," *17th Power Systems Computations Conference*, 2011.

[6] J. L. Mathieu and D. Callaway, "State estimation and control of heterogeneous thermostatically controlled loads for load following," *Hawaii International Conference on System Sciences*, pp. 2002–2011, 2012.

[7] C. Perfumo, E. Kofman, J. H. Braslavsky, and J. K. Ward, "Load management: Model-based control of aggregate power for populations of thermostatcally controlled loads," *Energy Conversion and Management*, vol. 55, pp. 36–48, Mar. 2012.

[8] S. Kundu, N. Sinitsyn, S. Backhaus, and I. A. Hiskens, "Modeling and Control of Thermostatically-Controlled-Loads," *17th Power Systems Computations Conference*, 2011.

[9] R. Malhamé and C. Y. Chong, "Electric load model synthesis by diffusion approximation of a high-order hybrid-state stochastic system," *IEEE Transactions on Automatic Control*, vol. 30, no. 9, pp. 854–860, Sept. 1985.